Biosensors and Bioelectronics 68 (2015) 371–381

Contents lists available at ScienceDirect

Biosensors and Bioelectronics

journal homepage: www.elsevier.com/locate/bios

A near infrared holographic glucose sensor

Evangelia Vezouviou *,[1], Christopher R. Lowe

Department of Chemical Engineering and Biotechnology, University of Cambridge, Tennis Court Road, Cambridge CB21QT, UK

ARTICLE INFO

Article history:
Received 10 August 2014
Received in revised form
15 December 2014
Accepted 3 January 2015
Available online 5 January 2015

Keywords:
Biosensor
Diabetes
Glucose
Holography
Chitosan
Near Infrared

ABSTRACT

Real-time glucose monitoring has been beneficial in reducing health complications associated with diabetes as well as a decrease in mortality. This report describes a novel holographic platform, fabricated via laser ablation on chitosan hydrogel with gold nanoparticles with a replaying in visible and near IR. The sensor responded with a 12 nm and 7 nm shift in wavelength at glucose concentrations in the 0–70 mM range and in the visible and near IR, respectively, at pH 7.4 and an ionic strength of 154 mM. The sensor did not respond to potential interferences found in the interstitial fluid, such as fructose, vitamin C and lactate, at their respective normal concentrations and was stable to fluctuations in temperature, pH and ionic strength. The characteristics of this sensor suggests that it may be applicable for use as an implanted device for the real time monitoring of glucose concentrations in the interstitial fluid using near IR as the interrogating medium.

1. Introduction

Diabetes *mellitus* is a chronic endocrine disorder with a prevalence of 347 million people worldwide, a figure that it is estimated to be the 7th leading cause of death by 2030 (Organisation, 2013). It is characterised by a down-regulation in signalling, response, or availability of the hormone insulin, leading to abnormal glucose levels. Normal blood glucose concentrations are maintained with the action of the hormone insulin at 3.5–8.0 mmol/L and Interstitial fluid (ISF) glucose concentration within the range 0.17–3.51 mmol/L depending on the body location (Kumar, 2005; Regittnig, 2003). Theoretical models for continuous glucose monitoring predict a 5-year increase in a patient's lifespan, 8 more years of sight and 6 years free from kidney disease and amputations, with a decrease in excess mortality for diabetic patients (Brimelow, 2013; Vaddiraju et al., 2010). A real-time glucose sensor will offer a more descriptive and accurate map of metabolic changes that will assist the clinician in prescribing a more reliable and precise insulin administration regime, a schematic proposal of patient's lifestyle and choices for maintaining their blood glucose concentration (Chia and Saudek, 2004; Michael and Boyne et al., 2003). In addition, implementing access to healthcare information via remote mobile devices (smart phones) allows a discrete, confidential and immediate communication between the patient and the clinician irrespective of location (Dimitrov, 2013).

At present, most commercially available real-time subcutaneous glucose measuring devices in Europe are enzyme-based electrochemical sensors (Sparacino and Cobelli, 2010; Gifford, 2013; McGarraugh, 2009; Rossetti et al., 2010). However, their market use has been limited by their short lifespan, the discomfort, the need for daily calibration, temperature fluctuations influencing enzyme activity, as well as foreign body response (Mou, 2010; Nichols et al., 2013). Overall, electrochemical sensors are positively characterised for their practicality in use; however, scope remains for other approaches to overcome obstacles faced with this type of sensor. Optical sensors measure photons and have the advantage over electrochemical methods in situations where patients have other conditions, such as those having pacemakers or cancer patients undergoing therapies with strong electromagnetic fields (Steiner and Wolfbeis, 2011).

Optical glucose sensing has been approached with boronic acids as recognition elements, (Garza et al., 2013; Gifford, 2013) where depending on the substituent structure (i.e. size and water solubility), are characterised by low toxicity and this was confirmed by *in vitro* (Wu Z et al., 2011) and *in vivo* (Konno, 2007) experiments. Although they have been criticised for non-specifically binding hydroxyl containing compounds, the concentration of such structures in the interstitial fluid of the subcutaneous space is substantially lower than the glucose concentration, (Huttunen, 1971; Ino et al., 2005; Ellmerer et al., 1998; Kawasaki and Yamanouchi, 2002) making boronates attractive agents for the purpose of this study. Furthermore, optical sensors based on boronic acids measure glucose by an equilibrium-based principle, in contrast with glucose consumption by a typical enzyme-based sensor which influences the glucose concentration in the

* Corresponding author.
E-mail address: Evangelia.vezouviou@cantab.net (E. Vezouviou).
[1] Dr. Evangelia Vezouviou is currently working at Philips Research, 101 Science Park, UK.

http://dx.doi.org/10.1016/j.bios.2015.01.014
0956-5663/

surrounding tissue and thus affects the glucose diffusion gradient and increases the lag time (Kumosa et al., 2010; Gifford, 2013). However, optical approaches based on coupling fluorescence-based sensing by coupling fluorescent derivatives to boronic acids suffer drawbacks such as photobleaching, instability in physiological conditions and fluorophore toxicity (Garza et al., 2013; Gifford, 2013).

Recently, holograms have attracted much attention as analyte-sensitive optical systems due to their robustness, versatility and ease of manufacture. They have the advantage of reporting the response by the means of a wavelength shift and/or intensity change (Saxby, 2004). Additional advantages of a holographic glucose sensor is that there is no requirement for a re-chargeable power unit co-implanted in the skin that is required by some other glucose sensors, (Kumosa et al., 2010) because the transduced signal is generated by reflected light and also that they do not photobleach thus avoiding the drawbacks of labels, such as fluorophores (Jin et al., 2009).

Moreover, a further advantage of boronic acid–based glucose sensors over the conventional enzyme systems is that boronic acids do not require co-substrates to react with glucose; however, the interaction between boronic acid and glucose is governed by the pH of the solution (Yan et al., 2004; Springsteen, 2002) and is related to the pKa of the receptor (Gierczyk et al., 2013; Yan et al., 2004). Fortunately, careful selection of a boronic acid analogue can overcome this challenge. Previous research in holographic glucose sensors has demonstrated glucose sensing at physiological pH using acrylic-based holograms modified with the 3- and 2-acrylamido-phenylboronic acid receptor (Kabilan et al., 2005; Yang et al., 2007). Implantation of these acrylic holograms could be problematic owing to potentially toxic leachates and the limitation of their replay wavelength in the visible region; therefore, it would be beneficial to fabricate a hologram with a replay wavelength that is able to penetrate the skin. An ideal wavelength for skin penetration by light is the long visible and near IR region, 600–1000 nm as it offers decreased scattering and low absorption by tissue chromophores or water (Cunningham, 2010) and without damaging the tissue. (Oliver, 2009; Nichols et al., 2013).

To achieve the characteristics required for fabricating a robust optical device for implantation, a volume holographic platform was designed based on biocompatible and biodegradable materials, such as chitosan, modified with a glucose sensitive phenylboronic acid receptor. The hologram was fabricated to replay in the visible and near Infrared region of the spectrum. The matrix was crosslinked with glyceraldehyde, and the holographic transduction introduced via laser ablation of gold nanoparticles generated *in situ* by chemical reduction of gold salts. The boronate receptor, 4-formylphenylboronic acid (4-FPBA), was selected since it binds glucose reversibly at physiological pH values and it was readily attached on chitosan backbone via a reductive alkylation. The 4-FPBA-chitosan hologram was assessed for its response to changes in the pH, ionic strength and temperature, likely to be experienced *in vivo* and parameters such as the degree of crosslinking adjusted to ensure little or no response under those conditions. This report demonstrates the holographic detection of glucose in a chitosan hologram fabricated with gold nanoparticles and monitored in the visible and near IR wavelengths.

2. Experimental section

2.1. Materials

All analytical grade reactants were purchased from Sigma-Aldrich, and methanol from Fischer Chemical. D-(+)-glucose, sodium chloride, D,L-glyceraldehyde, (+)-sodium L-ascorbate crystalline, gold (III) chloride trihydrate, chitosan (practical grade, degree of deacetylation 88%), glutaraldehyde solution, 3-aminopropyl triethoxysilane, tween 20, 4-formylphenylboronic acid, sodium L-lactate and L-ascorbic acid were purchased from Sigma-Aldrich. Sodium thiosulphate (Hypo) was purchased from Fischer Chemical. Microscope slides, super premium, 1.0–1.2 mm thick/plain 26 × 76 mm, were purchased from VWR International. The buffers were prepared according to the website http://www.liv.ac.uk/buffers/buffercalc.html and were made with deionised water at room temperature (22–23 °C). Adjustments to the desired pH values were reached by dropwise addition with HCl and/or NaOH and the ionic strength adjusted to 154 mM with the addition of NaCl. The glucose solutions were prepared in PBS (pH 7.4, 154 mM ionic strength).

2.2. Functionalization of glass slides

Sigma Aldrich protocol was followed for the aminosilanisation of glass slides with 3-aminopropyl triethoxysilane. Further aldehyde functionalization of the aminosilanised slides was as follows: The aminosilanised slides were exposed to glutaraldehyde solution (0.5% (v/v) in 70% (v/v) ethanol/dH_2O) for 5 min to facilitate crosslink sites for attachment of the chitosan's primary amines. The slides were then rinsed with dH_2O and left to dry.

2.3. Fabrication of chitosan holograms with gold (III) chloride trihydrate solution with a visible replay

The fabrication process in volume holographic gratings proceeds as follows: The coherent laser light wave propagates through the sensitive transparent suspension matrix and the reference wave travelling from the emulsion (at an angle from the mirror that the original wave strikes) create constructive interference (interference patterns-Lippmann layers) when they meet inside the emulsion and record the information within the polymer in a three-dimensional distribution (Bjelkhagen, 1998; Denisyuk, 1972; Saxby, 1994) (Scheme 1). In a metal nanoparticle treated matrix, upon laser irradiation, the nanoparticles align parallel, i.e. in fringes, and are spaced by an approximate distance of half the wavelength of the laser light they were exposed to (Kabilan et al., 2005). The fabricated Bragg grating when illuminated with white light, it reflects the double wavelength of the

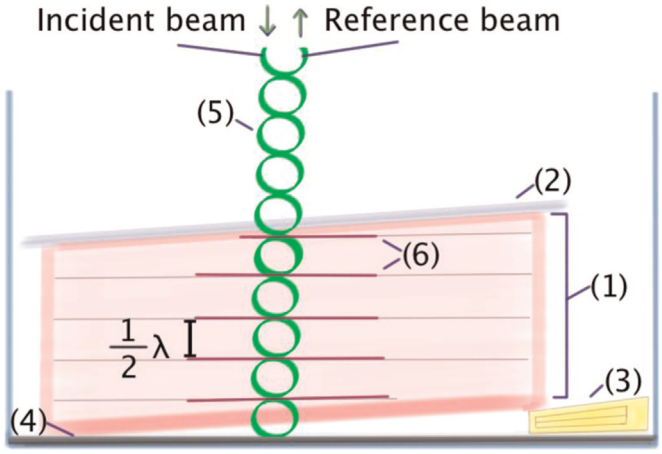

Scheme 1. Holographic fabrication. A photosensitive emulsion (1) coated on a glass slide (2) is placed inside a tray with a 7° spacer (3) and facing towards a reflecting mirror (4). Upon exposure to the laser irradiation (5), the gold nanoparticle grains are arranged in fringes (6) align in parallel to the surface of the polymer, and are separated by half the distance of the wavelength they were exposed to. The diagram is not to scale.

fringe spacing, filtering out other wavelengths of the white light; thereafter, recreating the monochromatic light that the matrix was initially exposed to (Graham, 2004; Kabilan et al., 2005). The distance of the fringes determines the characteristics of the grating in relation to the periodic perturbation of the refractive index insight the medium. The advantages of angular directional selectivity, refraction of specific monochromatic wavelengths on illumination with white light, and the absence of surface gratings are characteristic properties of true deep Denisyuk holograms that distinguish them from two dimensional surface holograms (Denisyuk, 1968).

Moreover, hydrogels can accommodate high affinity water molecules due to the polarity of monomer segments in their structure, where swelling or contraction depends on their chemical composition and surrounding environment (Ley et al., 1997): Thereafter, holographic fabrication in a receptor-treated hydrogel can lead to the advantage of realising the volumetric changes, in response to analyte-receptor interaction (binding), in terms of a wavelength shift (measured with a spectrophotometer).

A chitosan concentration of 2% (w/v) was dissolved in 1% (v/v) acetic acid/dH_2O and mixed thoroughly with a stirrer in a glass bottle for 24 h at 22–23 °C. The chitosan solution was then deposited on treated slides and spread with a Mayer rod no. 50. The coated slides were then exposed to warm air from a Philips air dryer (45 °C) until dry. The slides were then allowed to settle at room temperature and crosslinked with 0.1 M glyceraldehyde in 70% (v/v) ethanol/dH_2O for a period of 2 min. The crosslinked hydrogels were washed with 70% (v/v) ethanol/dH_2O and were placed at an angle of 45° degrees until dry. The gold chloride solution and hologram were prepared as follows: (1) Gold chloride trihydrate solution of pH 4.5 was diluted in dH_2O with a concentration 0.03 M, and 300 µl of the dissolved metal salt was placed in a petri dish. (2) Chitosan hydrogels were immediately placed in the petri dish with the polymer facing down, facilitating solvent diffusion into the polymer for approximately 1 min. (3) The slides were gently and rapidly washed with dH_2O and immediately immersed in 1 M sodium ascorbate solution for 1 min; the surface of the slides was gently swiped with a cotton rod to remove residual nanoparticles developed on the surface of the hydrogel. (4) After 2 min of exposure to the reducing agent, the slides were removed from the solution and washed thoroughly with dH_2O. Nanoparticle development can be observed immediately with the naked eye as a film colour change. (5) The slides were then immersed for 2 s in sodium thiosulphate and washed again with dH_2O on 45° degree stand. (6) After drying at 22–23 °C, the slides were then immersed in PBS (154 mM ionic strength and pH 7.4). Drying in various stages in the preparation of the hologram has been found to be an influencing parameter on the stability of the system and is an essential procedure. (7) The treated slides were then exposed to laser ablation. The equipment required included a Frequency-doubled Nd:YAG laser (532 nm) purchased from Brilliant Q, Quantel, Les Ulis, France, a Quartz spreader lens (focal length 8.8 cm) for laser ablation and three green dichroic front surface laser beam optical filters, purchased from Edmund optics Inc, NJ 08007-1380 USA. (8) Re-excitation of the embedded pattern with white light results in reconstruction of the hologram. The fabricated holographic films were gently cut with a scalpel to avoid anisotopic film tearing and then cut with a diamond cutter to the desired cuvette size. Measurements of the holographic response were obtained following vertical placement of the holographic grating in the platform and aqueous solution was added with a pipette to a volume of ~1.5 ml. The spectrophotometer for holographic measurement in the visible wavelength was an Avaspec ULS 2048-SPU2 with a grating range of 360–860 nm.

2.4. Fabrication of a chitosan hologram with gold (III) chloride trihydrate solution with a replay wavelength in the near IR

The Bragg equation $\lambda = 2nd\sin\theta$ governs the holographic replay and intensity (brightness); altering one of the constants in holographic fabrication such as the average refractive index (n), the distance between the fringes (d), and the angle of incidence (θ) (located between the incident ray propagation direction and the diffractive planes) (Kabilan et al., 2004) leads to altering the replay wavelength. Aminosilanised slides coated with 2%(w/v) chitosan solution [or chitosan-4-FPBA (33% and 50% of receptor/chitosan), depending on the procedure] were crosslinked with 0.01 M Glyceraldehyde for 2 min as described earlier, washed and dried and then exposed to 0.03 M gold chloride trihydrate solution. On this occasion, the slides were then gently and rapidly washed with dH_2O and immediately immersed in ascorbic acid solution (1 M) for 1 min; the surface of the slides was gently swiped with a cotton rod to remove residual nanoparticles developed on the surface of the hydrogel and then washed with dH_2O and left on a 45° stand to dry. The slides were not immersed in Fix solution (sodium thiosulphate) that was normally used to remove undeveloped metal salt as described previously. After the drying procedure at 22–23 °C, the slides were immersed in PBS (154 mM ionic strength, pH 7.4) for ~2 h to prepare the slides for subsequent measurements and allow further development of the nanoparticles in solution as well as further nanoparticle development during laser ablation for refractive index modulation. The slides were exposed to laser ablation in PBS. Briefly, the laser had a Flashlamp-Q switched delay 258 µs, 530 nm and approximately 300 mJ energy output and the slide was rotated by 7° to the mirror plate so that it was polarized at an angle to the laser pulse (ablation) of incidence. The slides were incubated in PBS for approximately 10 min after laser ablation to allow further nanoparticle modification. When the desired wavelength was obtained, the holograms were immersed in fix solution for 2 s, washed thoroughly with water and immersed in PBS. The fix buffer was used to avoid issues with the stability of the sensors by stopping further nanoparticle development and thus resulting in irreversible redistribution of the nanoparticles to keep the wavelength and replay intensity constant. Before the glass slides coated with the hologram were cut with a diamond cutter to the desired size, the films were first gently cut with a scalpel to avoid anisotopic film tearing. Measurements of the holographic response were obtained following placing the holographic grating vertically in the platform and adding the aqueous solution with a pipette to a volume of 1.5 ml. The spectrophotometer for holographic measurement in the near IR wavelength was an Avaspec Avantes ULS 2048xH-Spu 2, with a grating range of 600–1100 nm. The spectrophotometers and the spectrophotometric platform were purchased from Knight photonics Ltd., UK.

2.5. Synthesis of a 4-Formylphenylboronic acid chitosan hologram for glucose sensing

The attachment of 4-formylphenylboronic acid to chitosan was performed by adapting the procedure described previously (Reem Smoum and Srebnik, 2006). The synthesis and purification of the chitosan- 4-formylphenylboronic acid conjugate (chitosan-4-FPBA) was conducted as follows. Solution A: Chitosan (2 g) was dissolved in 200 ml of 1% (v/v) acetic acid, and the mixture stirred for 1 h to obtain a 1% (w/v) solution. Solution B: 4-Formylphenylboronic acid (2 g) was dissolved in 120 ml methanol to obtain a ratio of the solution A:B of 1:1 (w/w) resulting in 50% (w/w) of receptor. The experimental procedure was repeated, replacing Solution B with 1 g, and resulting in 1:0.5 (w/w) of chitosan:4-FPBA), i.e. in 33.33% (w/w) of receptor. The molecular

weight of chitosan polymer is not known and hence the ration of chitosan with the receptor moiety is represented as weight per weight (w/w). Once both solutions were dissolved at 22–23 °C, they were mixed together (Solution C) for approximately 1 h. The mixture was then washed with methanol, 2 M NaOH and dH_2O. Solution D was composed of 1.6 g of $NaBH_4$ and was dissolved in 150 ml methanol**. Solution C and D were mixed and left on a stirrer overnight at 22–23 °C. The next day, the precipitate formed and the solution was filtered to remove excess solvent and then washed with ethanol and water, and collected. Thorough washing of the product to remove residual unattached boronic acid molecules was essential. The collected precipitate was added to 1.5 ml tubes and samples were freeze-dried and the total weight of the dried samples was 1.71 g. The percentage recovery can be calculated by dividing the 1.71 g product weight by the weight of the initial chitosan. Recovery (%)=[1.71033/ 2 g "weight of 88% deacetylated chitosan"] x 100=85.5%.

**Safety consideration: The reaction between $NaBH_4$ and methanol results in the release of hydrogen. Consider mass of reactants and keep away from flame sources.

2.6. Fabrication of chitosan-4-formylphenylboronic acid hologram with gold (III) chloride trihydrate

The chitosan-4-FPBA conjugate (2% (w/v)) was dissolved in 1% (v/v) acetic acid at 70 °C on the stirrer for approximately 2 h. The solution had an approximate pH of 4.5. The mixture was then spread on treated glass slides and dried with warm air. It was left to settle at 22–23 °C and was thereafter crosslinked with 0.1 M Glyceraldehyde for 2 min, and washed thoroughly with 70% (v/v) ethanol/dH_2O and let standing at 22–23 °C until dry. It was exposed to a gold chloride solution of pH 5 for ~1 min and the procedure described above for hologram production followed.

2.7. ^{11}BNMR analysis of glucose binding to 4-formylphenylboronic acid as a function of pH

4-FPBA of concentration 30 mg/ml was used for the pH titration analysis and was diluted in 20% (v/v) of 1% (v/v) acetic acid/dD2O/ 80% (v/v) of 40% (v/v) ethanol/dD_2O. Dropwise addition of HCl and NaOH was performed according to the desired pH value and the volume was thereafter completed with D_2O. A solution of 4-formylphenylboronic acid (0.2 M) and glucose (0.2 M) was made in a 1:1 ratio. The boronic acid was dissolved in absolute ethanol and D_2O (60% (v/v)) while glucose was dissolved in D_2O. When the solutions were mixed, the pH was adjusted with 0.2 M NaOH and HCl and was made up to volume with D_2O. A final concentration of 30 mg/ml was obtained. NMR measurements were carried out with Brüker Avance 500BB ATM spectrometer, used with the IconNMR software for data acquisition. The NMR tubes used for the analysis were Wilmad 528PP made of Pyrex; the tubes were run with D_2O to confirm the non-overlap of the boron content of the tubes (minimal) with the samples and the background signal noise was subtracted from the data. The ^{11}B spectrum was run for 256 scans and the data were plotted using SigmaPlot 12 software.

2.8. ^{1}H, ^{13}C, ^{11}B NMR analysis of chitosan and chitosan-4-formylphenylboronic acid

A solution of 2% (w/v) chitosan or chitosan-4FPBA conjugate was dissolved in 2% (v/v) deuterated acetic acid/dD_2O and the spectra were run at 70 °C. The pH of the solution was measured to be 4.5 to avoid precipitation. The spectra were run on a Brüker Avance III 400 MHz instrument with a 5 mm QNP Cryoprobe at 298 K. The ^{1}H spectrum was run with pre-saturation of the D_2O signal to improve the signal-to-noise ratio of the sample peaks, with 64 scans. The ^{13}C spectrum was run for 2048 scans and the ^{11}B spectrum was run for 256 scans. The acquired spectra were then analysed and interpreted with the MestReNova NMR suite software (version 8.1.2), purchased from Mestrelab (Mestrelab Research, Santiago de Compostela, Spain).

Chitosan ^{1}HNMR [representing glucosamine monomer: OH–C (5.03 ppm), OH–CH–C (3.35, 3.66, 3.68, 3.70, 3.72, 3.75 ppm) –CH–N (3.35 ppm), $–H_2N–C$ (2.05 ppm)], [representing N-acetylglucosamine monomer: $CH_3–C=O$ (2.05 ppm)
^{13}CNMR [representing glucosamine monomer: OH–C (59.76 ppm), H_2NH**C** (55.67 ppm)
Chitosan-4FPBA ^{1}HNMR [representing glucosamine monomer: CH–OH (3.62 ppm), H_2NCH (substituted)], [chitosan-4FPBA link: Aromatic protons (7.24, 7.37, 7.38, 7.39, 7.66, 7.71, 7.73 ppm), $Ar–B–(OH)_2$ (1.84 ppm), $CH–NH–CH_2–Ar$ (2.27 ppm), $CH–NH–CH_2–Ar$ (3.64 ppm), $CH–NH–CH_2–Ar$ (3.05, 3.45 ppm), $CH_3–COO–NH$ (1.91, 1.93 ppm)]
Chitosan ^{13}CNMR [representing glucosamine monomer: OH–C (59.76 ppm), H_2NH**C** (55.67ppm)]
Chitosan-4FPBA ^{13}CNMR [representing glucosamine monomer: HC–O–CH close to boronic acid (97.43 ppm), CH_2OH (60.57, 70.02 ppm), H**C**NH (60.57 ppm), **C**NH_2 (55.99 ppm), $O=C–CH_3$ (177.33, 174.56 ppm), $O=C–CH_3$ (19.62–22.02 ppm)], [chitosan-4FPBA link: Aromatic carbons (129.29, 133.30, 133.69,134.36 ppm), NH–CH–Ar (50.51, 51.20 ppm)
Chitosan-4FPBA ^{11}BNMR: 19.27 ppm (pH 4.5, CD_3COOD)

3. Results and discussion

3.1. Fabrication of holograms based on biocompatible and biodegradable materials: Physiochemical characterisation and response

Chitosan holograms were fabricated initially with silver nanoparticles, utilising laser ablation (results not shown); however, their questionable toxicity and potential cause of argyrosis (Panyala and Havel, 2008) lead to the introduction of gold nanoparticles instead. The SEM and TEM analysis of the chitosan hologram fabricated with gold nanoparticles revealed a smooth surface, an approximate height of 1 μm in the xerogel state and nanoparticles in the size range of 5–20 nm arranged in apparent fringes (supplementary material). The different sizes may be owned to the different treatments applied to the polymer, chemical and optical (laser ablation) modification of the nanoparticles.

3.2. Parameters controlling the volume of the hologram

The pKa value interpolated from the pH range 3–10 was 5.5–5.7, compared to a literature of ~6.5 (Rinaudo and Desbrieres, 1999). The chitosan hydrogel was cross-linked by exposure to 0.1 M glyceraldehyde for 2 min or 5 min. The apparent pKa values suggested a higher amine substitution and stiffened elasto-mechanical properties with increasing cross-linker exposure time.

Crosslinking conditions were finally selected to be effected with 3 min of exposure to 0.1 M glyceraldehyde. Notably, the response of the hologram displayed little response (± 1 nm shift) to pH over the physiological range of 7.2–7.7. Similarly, the hologram showed little response to ionic strength (± 2 nm) in the physiological range of 50–200 mM, but contracted with increasing concentrations in the range 200–600 nm. The temperature response at pH 7.4 of the holographic system over the range 0–50 °C showed the hologram was stable, particularly over the physiological values (30–42 °C). It is noteworthy that the holograms with a

replay in the visible wavelengths were comparable to those with a replay in the near IR, although the individual near IR holograms showed overall stability, the reproducibility of the original starting diffraction wavelength varied, possibly attributable to the variable concentration of gold nanoparticles and overall treatment of the individually exposed slides. Nevertheless, the near IR grating produced in this study possessed angular selectivity and specificity that approximately aligned with the terms of Bragg's grating.

Thereafter, measurements were made with holograms that had <50 nm difference in starting wavelength. The original diffraction wavelengths in a typical bench production batch in the near IR, showed that the procedure results in an approximately 100 nm difference, i.e. a hologram may be produced in the range 700–800 nm, and on rare occasions ~900 nm. The initial wavelength appeared to be a function of the concentration of the nanoparticles. In future, this discrepancy could be minimised by strict control over the nanoparticle size and modification, and by further optimisation of the thickness of the recording medium in the pre- and post-ablation period, the solvent and chemical composition.

3.3. 4-FPBA modified chitosan hologram

With assurance that the baseline hologram was stable under physiological conditions, the platform was modified with a glucose responsive structure, initially 3-aminophenylboronic acid (3-APBA), which displayed a ~20 nm wavelength shift at physiological pH 7.4 and 10 mM of glucose; however, due to the slow release kinetics (upon PBS wash) and as the hologram did not present a full recovery to the original diffraction wavelength, with noticeable glucose remaining bound on the 3-APBA, studies were continued with an alternative receptor, 4-FPBA. Initial studies were undertaken in solution by ^{11}B NMR in order to establish the pKa of the receptor and to understand better its interaction with glucose.

3.4. ^{11}BNMR characterisation of 4-FPBA

The ^{11}B-NMR analysis showed peak shifts and accompanying changes in peak intensity (I) with increasing pH (Fig. 1). The stability of the ^{11}B-NMR data at values between pH 3–6 is indicative of the trigonal boronate species (Fig. 3 (1)). The peak shift from 28 ppm towards 21.82 ppm and thereafter (Fig. 1), observed at pH values between 7.4 and 10, is indicative of an increase in the concentration of the tetrahedral phenylboronate species and a negative charge on the receptor (Fig. 3 (3)): Importantly, the data shows the presence of both trigonal and tetrahedral conformation illustrated throughout the pH range (Fig. 1(B)).

The same experiment was repeated in the presence of glucose. The results showed a shift in the apparent pKa values from 7.8 to 7.5, in response to glucose binding, extrapolated from Figs. 1 and 2, respectively.

The chemical shifts ~28 ppm that appeared in all the samples, even at higher pH in Fig. 2, are likely to be in the trigonal form. Thereafter, glucose may bind to both the trigonal (Fig. 3 (3)) and the tetrahedral (Fig. 3 (4)) boronate conformation, resulting in ester formation, while glucose binding in the trigonal form may be more susceptible to hydrolysis.

The results of Fig. 1 may translate to I(1) being the trigonal form (Fig. 3(1)), while I(2) may represent the tetrahedral conformation (Fig. 3(2)). However, in the presence of glucose more than two conformations were indicated, marked as horizontal rows a, b, c and d in Fig. 2. In relation to Fig. 1 it is suggested that row a in Fig. 2 may relate to the trigonal conformation, while row b to the trigonal conformation bound to glucose, while rows c and d may account to the tetrahedral boronate conformation *per se* and bound to glucose, respectively. Glucose binding to the tetrahedral boronate is assumed to commence at pH 5, according to Fig. 2 (row c). Additionally, in the presence of glucose there is an increment in both the trigonal confirmation as well as the tetrahedral forms of boronic acids and boronic esters. Thus, results obtained with the 4-FPBA pH titration curves (Figs. 1 and 2) suggest a pH dependent interchange of 4-FPBA between the trigonal and tetrahedral forms, as illustrated in Fig. 3, where the prevalence of each depends on the pH and the presence or absence of glucose. The results also agree with assumptions that the conformational forms of boronic acids in solution are in equilibrium. (Springsteen,

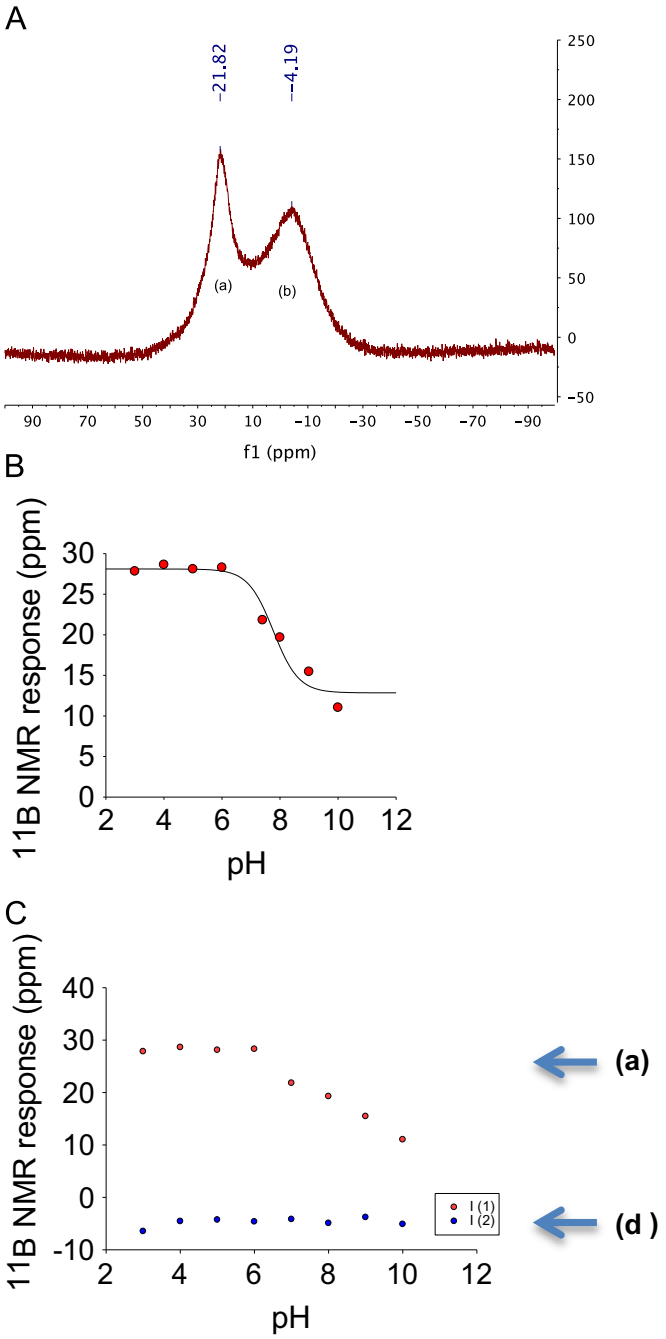

Fig. 1. Solution ^{11}B NMR spectroscopic pH titration curve of 4-FPBA. A typical ^{11}B NMR spectrum of pH 7.4 (A) indicates two peaks with different intensities, I(1) at (a) 21.82 ppm and I(2) at (b) −4.19 ppm. The data plotted in (B) represent the ^{11}B peaks with the highest intensity (I(1)). (C) illustrates the ^{11}BNMR peaks of the analysed samples at each pH value. The peaks with the highest intensity are in the order of (I(1)) > (I(2)). The apparent pKa value, 7.8, was obtained with SigmaPlot software.

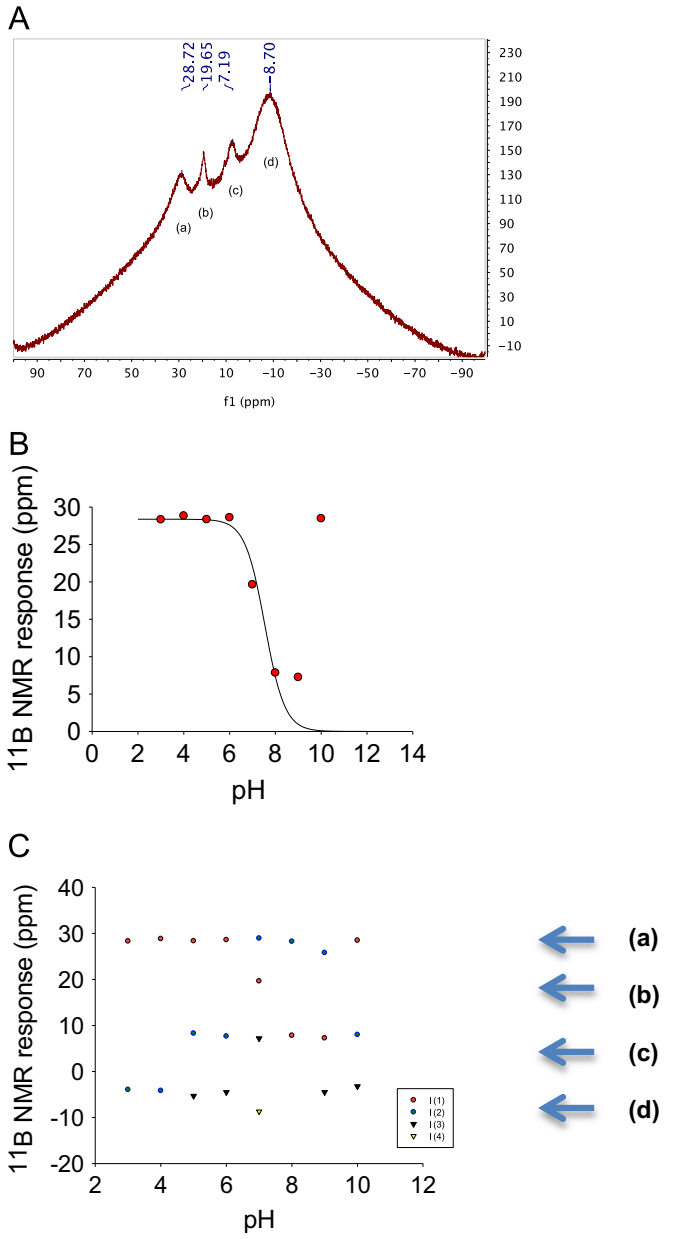

Fig. 2. Solution ^{11}B NMR spectroscopic pH titration curve of 4-FPBA in the presence of 100 mM glucose. A typical ^{11}B NMR spectrum of pH 7 (A) indicates four peaks with different intensities, I(1) at (a) 28.72 ppm, I(2) at (b) 19.65 ppm and I(3) at (c) 7.19 ppm and I(4) at (d) −8.7 ppm. The data plotted in (B) represent the ^{11}BNMR peaks with the highest intensity (I(1)). (C) illustrates the ^{11}BNMR peaks of the analysed samples at each pH value. The peaks with the highest intensity are in the order of (I(1)) > (I(2)) > (I(3)) > (I(4)). The apparent pKa value, 7.5, was obtained with SigmaPlot software. ^{11}B-NMR pH titration curve of 4-FPBA receptor in the presence or absence of glucose.

2002) Furthermore, the conformational structures in other ^{11}BNMR pH-depression experiments with 3-acrylamidophenylboronic acid are in approximate agreement with findings in this work (Sartain, 2008; Xiaoping Yang et al., 2006).

3.5. 4-FPBA-chitosan synthesis

The 4-FPBA analogue was selected in this work due to its lower pKa, 7.6, (Yan et al., 2004) and the feasibility of attaching it to the chitosan polymer via reductive N-alkylation. A series of experiments were performed in order to validate the attachment of the receptor to the polymer and to confirm its structural integrity. Although others have applied the 4-FPBA-chitosan conjugate for sensing analytes that included glucose (Matsumoto and Kondo, 2002; Shervedani, 2008; Reem Smoum and Srebnik, 2006; Asantewaa et al., 2013), this work is the first to use this conjugate for hologram fabrication. The ^{1}H, ^{13}C and ^{11}B NMR spectra of the synthesized product includes the chitosan skeleton and the conjugate, and essentially has additional resonances which ratify the reductive N-alkylation step, and thereafter confirm the synthetic route. Specifically, the primary amines of the synthesised conjugate are almost absent in positions whereas they appear in the NMR of the chitosan backbone, indicating that the substitution occurred most likely on the glucosamine moiety of the chitosan; the secondary amines of the N-acetylglucosamine seem to be untouched, as confirmed by the appearance of the acetyl group protons and carbons in the analysis, and this additionally supports the part acetylation of the polymer. The primary amine protons are replaced by the linkage of the primary amine protons of the conjugate in both ^{1}H- and ^{13}C–NMR CH–NH_2–CH–Ar and of the CH–NH_2–CH–Ar. The resonance peaks of the aromatic group were also apparent as well as the conformational structure of the receptor with ^{11}B–NMR. This can be justified by the fact that the pH of the solution used for the NMR analysis was relatively low (pH 4.5) as the solvent used to dissolve the conjugate was 2% (v/v) acetic acid; thus, it may have influenced the charge on the amines in the polymer, which may have thereafter affected the structural conformation of the receptor: In relation to the in solution ^{11}BNMR experiments of the receptor, in the absence or presence of glucose at pH 4-5 (~28 ppm), the resonance peak of the chitosan-4-FPBA conjugate at pH 4.5 (19.27 ppm) correlates with the transition towards the tetrahedral confirmation and indicating possible interaction with the aminosugars on the chitosan backbone.

The mass spectrometry analysis of chitosan polymer and the synthesized chitosan-4FPBA conjugate was performed with negative ion electrospray MS; however, no firm conclusions can be drawn due to the complex structure of the polymer. The presence of the boron linked on the chitosan polymer was also established with confocal microscopy: Solutions of chitosan and the conjugate and a conjugate-based hydrogel were examined for their fluorescence, in the presence and absence of Alizarin Red S (ARS), according to the standard in solution technique used for the ARS- boronic acid binding constant determination (Springsteen, 2002), with modifications. The appearance of fluorescence (λ_{em}~588 nm) validated the attachment of the receptor to the chitosan. A picrylsulphonic acid assay (TNSB) was performed in order to compare the primary amine substitution of an uncrosslinked, a crosslinked and a 4-FPBA-modified crosslinked hydrogel where in the highest amine modification appeared as the least orange coloured film. Measurements were obtained by diluting stock 5% (w/v) TNSB solution to 0.5% (w/v): The three hydrogels, A, B and C were exposed to 300 µl of the diluted TNSB solution, at 22–23 °C. These analytical tests confirmed the fabrication of a chitosan-4FPBA hydrogel.

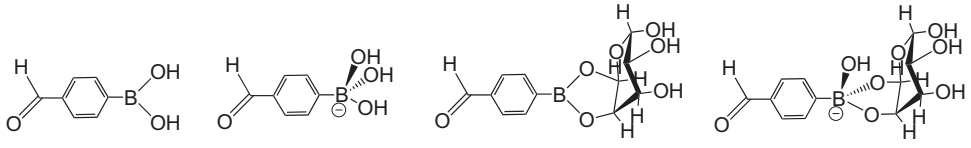

Fig. 3. Proposed structural conformation of 4-FPBA in trigonal (1) and tetrahedral conformation (2), and in complexation with glucose (3) and (4), respectively.

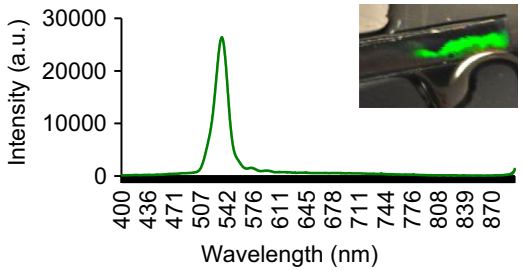

Fig. 4. Hologram produced with the chitosan-4-FPBA conjugate with a replay wavelength in the visible ~534 nm, 10 ms Integration time.

3.6. Holographic fabrication of chitosan-4-FPBA conjugate in visible and near IR

The hologram fabricated with the chitosan-4-FPBA conjugate illustrated in Fig. 4 has a holographic replay wavelength in the visible range with a very bright intensity.

Although a holographic flake (hologram detached from a surface, such as glass slide) was produced that is desirable for human implantation, at this point it was preferable for practical reasons to continue with measurements of a hologram attached to a glass slide. The pH titration curve of the receptor modified hologram in the absence or presence of glucose showed a pKa value of 6.3 and 6.5, respectively. The difference in the pKa value of the receptor-modified system with the chitosan holographic platform (pKa of 5.5–5.7) is likely to be due to the 4-FPBA modification of the chitosan backbone. The receptor-modified hologram was found to be chemically and physically stable under conditions that resemble those in the human body, such as temperature, ionic strength, and pH.

Moreover, communication with the subcutaneous space can be achieved externally by optical interrogation through the skin. A hologram with a replay in the visible range does not provide an adequate and readable signal through the skin, as the skin optical window lies in the near IR (Oliver, 2009; Nichols et al., 2013). Thus, it was necessary to fabricate a hologram with a wavelength replay originating in the near IR. Although others have considered investigating near IR holography for other purposes such as for holographic memory storage (Tarkka et al., 1994), with exposing the emulsion directly to near IR laser irradiation, almost all of these studies utilised chemical reagents harmful to the human body and the holograms were susceptible to photobleaching due to the use of photochromic dyes. Our study suggests that aggregation of the nanoparticles in the periodic grating could be used to offer optical modulation via refractive index changes and a coupling mechanism that includes resonant excitation of the surface plasmon resonance (SPR) waves via the holographic grating and subsequent photomixing (Aslan and Geddes, 2004; Smirnova et al., 2009; Hajdukova et al., 2007; Gaponenko, 2010). A probabilistic interpretation for the switch in the Bragg diffraction from visible to the near IR wavelength is the periodicity and distribution of the nanoparticles in fringes (i.e. aggregation) as well as the change in the refractive index of the hologram affecting the holographic replay with multiple coherent scattering, due to sodium thiosulphate acting as a modulating tool. The aggregation of the nanoparticles was confirmed with TEM analysis of the near Infrared hologram and was absent in the visible hologram (Supplementary material).

3.6.1. Optical modulation of holographic gratings

Generally, in a volume holographic grating, the interference light pattern induced by the applied electromagnetic field, encourages the spatial modulation of the photosensitive constituents of the emulsion (in the case of gold nanoparticles) with concurrent refractive index changes (Kogelnik, 1969), resulting in a concentration gradient difference, and thus to a volume grating which is directly related to the absorption constant and light sensitivity of the emulsion. The refractive index will vary sinusoidally based on the formation of alternating regions of high and low refractive index (Bendana et al., 2010; Rodrigueza and Butlerb, 2000; Šmíd and Keprt, 2004): Notably, a high refractive index difference between the white and dark fringes, accounts for the brighter holograms (Gaponenko, 2010; Graham, 2004) and this may be assumed by TEM analysis of the NIR hologram (supplementary material), which illustrates void spaces between an array of nanoparticles, that may represent the fringes. Talking in account the fact that quantum particles are considered as waves, when the particles travelling with the same energy (wavelength) face a potential step (such as a difference in the refractive index in the alternating fringes) they will experience partial reflection and partial transmission with simultaneous modification of the wavelength (Gaponenko, 2010): Light from upper and lower indices will interfere, and the phase matching of the waves regulates the degree of constructive or destructive interference. The constructive interference (two waves in phase) from the fringes is responsible for the holographic replay due to the interference of the incident and reflected waves that are in phase (Gaponenko, 2010). The thickness of the fringes (as well as the polymer) is also significant for the propagation distance of the evanescent waves to reach the surface (Cho, 2010; Cowan, 1972; Ozakl and Kawata, 2011; Monis, 2010) and contributes to wavelength modification. Thus, the concentration of the nanoparticles in the fringes in the polymer affects the diffraction efficiency of the grating (Adleman et al., 2006) via refractive index modulation (Naydenova et al., 2005). The developed metal grains in the opaque fringes ultimately absorb most of the light (coherent laser or white lamp) that is interacting with them and they selectively scatter the rest in the form of standing waves of different potential energy (Bendana et al., 2010; Gaponenko, 2010; Saxby, 2004) thus the reflection efficiency of such fringes is similarly dependent on the characteristics of the metal particles and the fringe periodicity (as well as refractive index) which then influences the interference of the SPR on the holographic replay. The holograms with the near IR replay frequently required subbing in PBS in order to shift from the visible to the near IR.

3.6.2. Plausible explanations for the wavelength shift to near IR

There may be two plausible explanations, although both events relate to aggregation and the holographic replay (diffraction grating): (1) The superposition of continuous oscillatory functions in reciprocal space (Zanchet et al., 2000) due to events occurring in the post-fabrication period such the interplay between the SPR of the aggregated nanoparticles in the near IR and the interference pattern from the alternating refractive index fringes (Bragg grating). Assuming that "the total electric field within the structure is a sum of forward and backward propagating waves" (Rodrigueza and Butlerb, 2000) then it can be considered that upon white light illumination the fabricated holographic (visible wavelength) wave that is produced via the sinusoidally altered refractive index of the fringes can excite the SPR of nanoparticles in the near IR region (due to aggregation). However, only the ballistic photons (coherent photons reflected on material-characteristic features) which come from a certain depth are coherent with the reference beam (Mecher et al., 2002) and thus the SPR waves of the nanoparticles can interact with the reference beam of the hologram before they decay: Accordingly, it can be considered that the quantum-size effect of the optical and electronic properties of the nanoparticles (SPR) may play a role in the volume Bragg replay, this feature is supported by a study stating that a periodically ordered metal layer of nanoparticles in a medium can convert an incoming light wave to a surface Plasmon-polariton wave and vice versa (Cowan, 1972; Smirnova et al., 2009). Secondly, (2) due

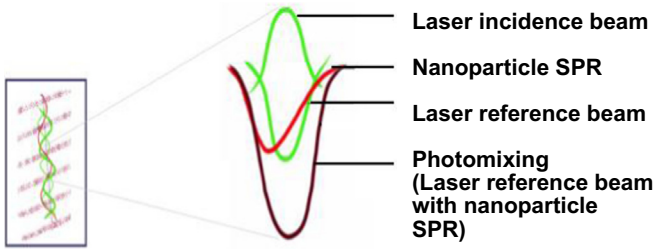

Scheme 2. Light photo mixing.

to the *in situ* interaction of the nanoparticle SPR (in near IR due to aggregation) with the object beam at the moment of laser exposure resulting in the photomixing of the two waves (object and SPR) and their constructive interference with the reference beam modulation of the refractive index (Scheme 2). The SPR of the nanoparticles can travel a short distance (~200 nm (Hong, 2012)) and then decay; thereafter, the monochromatic replay obtained cannot be considered solely an SPR replay as the cross section of a typical hologram (dry) analyzed in this study, indicated an approximate height of 1.2 μm (SEM analysis, Supplementary material). In addition, considering a uniform fringe spacing and mass modulation, it is possible that the SPR from the nanoparticles has the same wavelength (Hong, 2012) and thus interacts consistently throughout the volume of the grating. Moreover, due to the assumption that two different wavelengths interact, it must be expected to have a time travelling change, which although in a hologram of an object can result in image blurring, it should not make a difference for a hologram with no image display. Thereafter, an optical coupling platform for the free (void) space of the volume hologram can be used to decrease the speed of the evanescent wave to achieve interaction of the different light waves (Cowan, 1974), in this case, to couple the reference holographic beam reflected internally and the nanoparticle SPR: Chitosan matrix and an aqueous medium, i.e. PBS, may act as coupling platform. This last event can support both imprinting the near IR wavefront as the holographic replay as well as the stimulation of the SPR with the wavelength replay. Both cases are prone to be affected by a refractive index change that will modulate the light being absorbed, refracted or reflected. Consequently, the outcome of the SPR may rely on the polarisation dependence (monochromatic angle-dependent replay) of gratings recorded in films. Light beams carry spin angular momentum, which is associated with their polarization state, but also orbital angular momentum which is associated with the topology of wavefronts and phase singularities (Uchida, 2010). An increase in polarizability of the system drives a transition between suppression and emergence of diffraction features (Bendana et al., 2010). The fringes may act as dielectrics experiencing dielectric polarization when irradiated, and as the hologram was not fixed, the small nanoparticles could move freely and be attracted via electrostatic interactions by the larger nanoparticles and align to the laser radiation field to form aggregates and the fringes, thus depending on the polarizability of the laser. Consequently, the fringes can be considered in terms of refractive index modulation, dielectric phenomena and their SPR influence towards the wavelength replay. The incident light from the hologram or laser are both in a single polarized state, and thus the surface plasmon waves of the particles are selectively polarized and the excited waves depend on the characteristics of the nanoparticles such as aggregation. Moreover, based on diffraction theory, a particle illuminated with a propagating wave generates diffracted evanescent modes and conversely, based on the reciprocity theorem, a particle located in an evanescent field converts part of this field in to propagating waves (Vigoureux and Girard, 1992). Thereafter, laser ablation and/or the holographic replay may equally result in a change of the surface plasmon resonance and hence in light scattering of the nanoparticles. In support, photomixing of both cases and based on physics principles, if two wavelengths are "mixed", photons may interfere and this photomixing can result in a complex wave. In this case, if the sum of the two waves that have closely interfering crests will create the constructive interference, and the intensity will be the sum of their amplitudes due to the superposition of the waves.

3.6.3. *Holographic replay and SPR interaction*

In research based on plasmonic nanoantennas, it was observed that a transition of the dipolar plasmons in the result of interference between the wave reflected at the planar interface and the beam scattered from the spheres, which lead to phase shifts as the wavelength sweeped across the plasmon resonance (Bendana et al., 2010). This study supports the previous hypothesis that the interaction of the laser or the holographic replay light with the SPR causes a shift in the wavelength. SPR-enhanced Bragg gratings have also been suggested elsewhere in surface holograms and the degree of the intensity is thought to be indicative of the strength of the resonance (Cowan, 1974). It was also observed that the volume holograms received here with a near IR holographic replay possessed enhanced intensity compared to the ones prepared with a holographic replay in the visible wavelength. However, it is plausible that the brightness of the two systems, apart from possible sensitivity variations in the detector spectrophotometer devices, may be due to different reasons: For the visible region is accounted for by the perfectly aligned fringes and uniform total refractive index (benefit from the fix bath) while for the near IR is accounted for by the enhancement of the holographic replay with nanoparticle plasmon near IR resonance due to photomixing and concurrent average refractive index change (Scheme 2). It is known that when the gap between the two particles exceeds ~2.5 times the size of the particles it results in a decrease on the resonance event to almost zero (Aslan and Geddes, 2004), thus authenticating the data here (TEM analysis of holograms with replay in visible vs. NIR wavelengths, Supplementary material) and indicating that the enhanced excitation of surface plasmon resonance of the nanoparticles is due to the aggregation of the gold nanoparticles and is a characteristic of holograms with a near IR replay rather than with a hologram with visible replay wavelength (TEM analysis of visible hologram, Supplementary material). In addition, the scattering is based on the reflection coefficient of the nanoparticle layer while alterations can result in a phase shift (Takumi Sannomiya et al., 2010). Moreover, the coherent backscattering of the gold particles increases when it is surrounded by a shell of higher refractive index medium (Takumi Sannomiya et al., 2010), and this may account for the aggregated nanoparticles around the core. This hypothesis concludes that by varying the nanoparticle size and aggregation in the fringes it will lead to a sharp transition in the wavelength and it establishes a clear difference in the behavior of the holographic Bragg gratings. The dipole moments of the nanoparticles can be influenced both by the external wavelength and a wavelength induced by other particles at the lattice position and is additionally affected by refractive index where the light vector travels in material from one refractive index to another refractive index. It is known that when light passes through a medium of lower refractive index, then the wavelength becomes longer (Gaponenko, 2010) and thus there may have been a refractive index change in the post ablation period (via aggregation) that red-shifted the wavelength. While other groups have implicated the SPR interaction with holographic replay in different types of holograms (Ozaki and Kawata, 2011), particularly surface holograms, this study is the first to demonstrate the production of a hologram with a replay in the near IR in a volume hologram based on those assumptions. The findings presented in this work are important in the design of a near IR modifiable implantable sensing platform that opens the way to many biomedical and other sensing technologies.

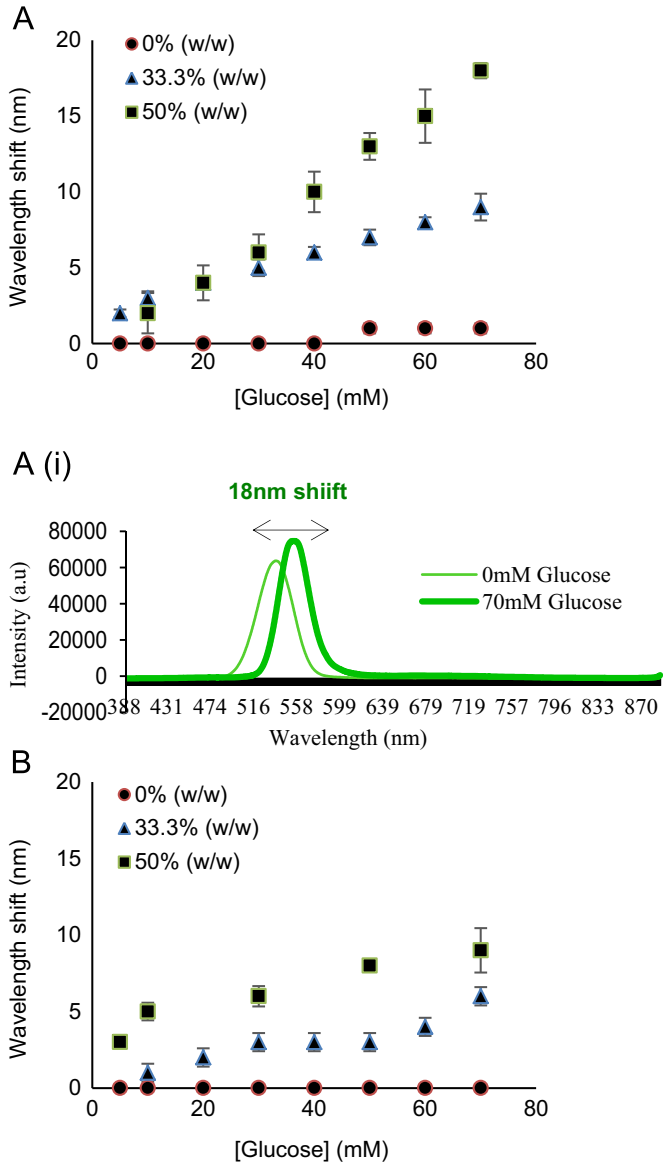

Fig. 5. Response of holograms replaying in the visible (A) and near IR (B) wavelengths, both fabricated in a 4-FPBA-chitosan hydrogel containing different receptor concentrations, in a range of 0%, 33.33% and 50% (w/w) of total weight of the mixture of receptor: chitosan, tested at various glucose concentrations in PBS, pH 7.4, ionic strength of 154 mM, 22–23 °C. PBS washing steps after the addition of each glucose concentration assured the return of the hologram to its initial wavelength value. The regression analysis for the best line fit were calculated for each graph with holographic response in the visible wavelength to have a linear equation of $y=0.1405x$ and $R^2=0.8942$ for 33% of receptor while for 50% a polynomial line $y=0.001x^2+0.1957x$ and $R^2=0.99194$ was selected as a better fit. Holographic near IR response gave a linear equation of $y=0.076x$ and $R^2=0.90547$ for 33% receptor while for 50% of receptor a polynomial equation was selected $y=-0.0027x^2+0.3094x$ and $R^2=0.8429$. A representation of the wavelength shift is given in A (i) [50% (w/w) 4-FPBA-chitosan hologram], glucose concentrations 0–70 mM with a replay wavelength ~530 nm and ~548 nm, respectively.

3.7. Holographic glucose sensing in the visible and near IR

The exposure of a boronate-treated hydrogel to a diol compound, such as glucose, creates a charge on the phenylboronate groups, allows more water molecules to influx via the Donnan potential and cause swelling (Hisamitsu et al., 1997) and hence wavelength shift. The data given in Fig. 5 represent the response of chitosan-4FPBA conjugate holograms fabricated with gold nanoparticles with replay wavelengths in visible and near IR wavelengths, and show an almost linear response as a function of glucose binding. The holograms in these experiments were washed with PBS between glucose concentration measurements to assure complete return to the initial wavelength. The response of the hologram with the chitosan-4-FPBA conjugate (Fig. 5) was reported to be reversible in both visible and near IR. Control experiments were performed on a chitosan hologram lacking the glucose recognition element and the hologram was unresponsive in the range of 0–40 mM and an increase in 1nm was observed in concentrations of 50–100 mM, confirming that the swelling observed with the chitosan-4FPBA conjugate holograms was due to glucose interaction with the receptor. The response of the biosensor to glucose addition was almost linear, and the wavelength shift increased with increasing glucose concentrations. Experiments performed on the kinetics and the swelling of the holographic sensor showed that it requires a longer equilibration time (~1/3x) compared to the total time required for deswelling. For example, at glucose concentrations of 5 mM, 20 mM, 40 mM the recorded total binding times to equilibration were approximately 6, 15, 38 min, respectively, while for the respective concentrations to reach wavelength baseline (total release time) was approximately 5, 5, 14 min (representative responses of Fig. 5 (A)). The difference in the wavelength shift between visible and near IR holograms may accounted for by the additional chemical modification for the near IR hologram and possibly the higher content of small nanoparticles (~5 nm) which may interfere with the receptor and block glucose from binding. Another possibility may be the stacking of the receptors that may occur as a result of the non-uniform distribution of the chitosan-4FPBA conjugate. As this is the first study to demonstrate glucose sensing with a hologram with a near IR replay, it remains in the future to adjust and increase the response of the near IR holographic biosensor.

In both the holographic systems, the binding response of the receptor with glucose was also influenced by the receptor and glucose concentrations (Fig. 5): Overall, the conjugated matrix with the highest degree of receptor substitution (Fig. 5) displayed stronger and more effective swelling of the system on glucose binding (50% of receptor) and thus was selected as the platform system for further evaluation of the receptor response to other potentially interfering analytes.

3.7.1. Principal interferences in the ISF composition and skin structure that may affect sensor responses

The diol-compound interference of seven molecules (D-glucose, fructose, vitamin C, sodium-L-lactate, N-acetylglucosamine, and glucosamine) was tested under physiological conditions. The holographic binding and release response appeared to be related to their reaction with 4-FPBA. Typical ranges of diol compound concentrations that may be reached in the interstitial fluid of the subcutaneous space were tested on the hologram and was found insensitive to display no response included: Fructose (0–20 μM), vitamin C (pH 7.4) (20–120 μM) and sodium-L-lactate (0.5–5 mM), at 22–23 °C, pH 7.4, ionic strength 154 mM. Measurements were conducted with holograms replaying in both the visible and near Infrared wavelengths and presented similar responses.

3.7.2. Future directions

Other structures, such as the breakdown products of the biodegradable hologram (i.e. glucosamine and N-acetyl glucosamine) may need further evaluation as their actual concentration *in vivo* is currently not known. Such an investigation can initially be performed with the use of chitosan-biodegradative enzymes (i.e. N-acetyl-β-D and N-acetylglucosaminidase, and chitosanase (Escott, 1995)), and will also provide insights into the rate of degradation in relation to the stability of the holographic replay and overall sensor. Furthermore, the biocompatibility of the system is

presumed and is based on the basic literature principles as well as with recent research advances from other groups that are addressing closely related outcomes in different systems: (Azevedo, 2011; Dyer et al., 2002; Honarkan, 2009; Huang, 2004; Cambre, 2011; Asantewaa et al., 2013; Pan et al., 2007) In relation, future scope includes the design of cytotoxic assays, which will provide further insights on the biocompatibility of the holographic platform.

4. Conclusions

The prototype holographic platforms based on biocompatible and biodegradable materials were successfully produced to replay in the visible and near IR. Such a platform is a powerful tool that can be further modified to sense other biological materials inside the human body, such as lactate for the prognosis of acute myocardial infractions. The 4-FPBA receptor-treated chitosan holograms could operate with an acceptable spectral response in the interstitial tissue, providing prospective *in vivo* application. It remains to enhance the sensitivity of the system in order to generate a higher wavelength shift in the low glucose concentrations found in the interstitial fluid. The results received from this pilot study appear promising, although further experiments are required to confirm that this system is suitable for implantation, such as *in vitro* evaluation in a cell culture.

Acknowledgments

Dr. Evangelia Vezouviou was a Ph.D. student at the University of Cambridge, Department of Chemical Engineering and Biotechnology, under the supervision of Professor Christopher R. Lowe, and was funded by EPSRC and Philips Research. The information on this paper formed a part of her Ph.D. thesis (Vezouviou, 2013). The authors would like to thank Dr. Jay Patel (Industrial supervisor, Philips Research) for helpful discussion, Dr. Peter Grice (University of Cambridge) for his assistance in NMR and Dr. Jeremy Skepper (University of Cambridge) for his assistance in SEM and TEM.

Appendix A. Suplementary Information

Supplementary data associated with this article can be found in the online version at http://dx.doi.org/10.1016/j.bios.2015.01.014.

References

Azevedo, E.Pd, 2011. Aldehyde-Functionalized Chitosan and Cellulose:Chitosan Composites: Application as Drug Carriers and Vascular Bypass Grafts. University of Iowa (Pharmacy.).
Bendana, X.M., Auguié, B., Barnes, W.L., García de Abajo, F.J., 2010. Diffractive arrays of gold nanoparticles near an interface: critical role of the substrate. Phys. Rev. B 82, 155447.
Zanchet, D., Hall, B.D., Ugarte, D., 2000. Estimating nanoparticle size from diffraction measurements. Appl. Crystallogr. 33, 1335–1341.
B Gierczyk, M.K., Schroedera, G., Sporzyńskib, A., 2013. NMR studies of boronic acids and their derivatives. N. J. Chem. 37, 1056–1072.
Garza J.T., Cummins B.M., Coté G.L., 2013. Limitations of current fluorescent glucose sensing assays based on competitive binding, Optical diagnostics and sensing XIII: Toward Point-of-Care diagnostics. 8591.
Bjelkhagen H.I., New recording materials for holography. 1998.
Brimelow, A., 2013. Diabetes: Excess Deaths Well Down, Study Indicates. BBC News: Health, BBC online.
Ley, C., Calderara, I., Lougnot, D.J., 1997. Holographic grating recorded in polymer hydrogels- an optical application as a sensor in aqueous environment. Measurement Sci. Technol. 8 (9), 997–1000.
Chia, C.W., Saudek, C.D., 2004. Glucose sensors: toward closed loop insulin delivery. Endocrinol. Metab. 33 (1), 175–195.
Cho, A., 2010. Century-Long debate over momentum of light resolved? Science 327, 1067.
Cowan, J.J., 1972. The surface plasmon resonance effect in holography. Opt. Commun. 5 (2), 69–72.
Cowan, J.J., 1974. Holography with standing surface plasma waves. Opt. Commun. 12 (4), 373–378.
Kumosa, L.S., Gough, D.A., Routh, T.L., Lin, J.T., Lucisano, J.Y., 2010. Function of an implanted tissue glucose sensor for more than 1 year in animals. Sci. Transl. Med. Home 2 (42), 42–53.
D D Cunningham, J.A.S., 2010. In Vivo Glucose Sensing (Chemical Analysis: A Series of Monographs on Analytical Chemistry and Its Applications). Wiley-Blackwell, New Jersey.
Denisyuk, G., 1968. The theory of deep holograms. Proceedings-Royal Society A 304 (1478), 275–289.
Denisyuk, G., 1972. Holography, 1948–971. Science 177 (4046), 299–313.
Dimitrov, D.V., 2013. Remote control in diabetes. Adv. Predict. Prev. Pers. Med. 3, 389–398.
Dyer A M, H.M., Watts, P., Castile, J., Jabbal-Gill, I., Nankervis, R., Smith, A., Illum, L., 2002. Nasal delivery of insulin using novel chitosan based formulations: a comparative study in two animal models between simple chitosan formulations and chitosan nanoparticles. Pharm. Res. 19 (7), 998–1008.
E Mecher, F.G.-G., Tillmann, H., Horhold, H.H., Hummelens, J.C., Meerholz, K., 2002. Near-Infrared sensitivity engancement of photorefractive polymer composites by pre-illumination. Nature 418, 959–964.
G M Escott, D.J.A., 1995. Chitinase activity in human serum and leukocytes. Infect. Immun. 65 (12), 4770–4773.
G Sparacino, A.F., Cobelli, C., 2010. "Smart" continuous glucose monitoring sensors: on-line signal processing issues. Sensors 10 (7) (7651-6772).
Gaponenko, S.V., 2010. Introduction to Nanophotonics. Cambridge University Press.
Gifford, R., 2013. Continuous glucose monitoring: 40 years, what we've learned and what's next. Phys. Chem..
S. Graham, Pract. Hologr.. 2004.(3rd Edition).
H Honarkan, M.B., 2009. Applications of biopolymers I: chitosan. Monatshefte für Chemie 140 (12), 1403–1420.
H Huang, X.Y., 2004. Synthesis of polysaccharide-stabilized gold and silver nanoparticles: a green method. Carb. Res. 339 (15), 2627–2631.
H Naydenova, S.S.M., Martin, S., Toal, V., 2005. Holographic recording in nanoparticle-doped photopolymer. Mater. Syst. Opt. Data Storage Processing, 6252.
Huttunen, J.K., 1971. Fructose in medicine: a review with particular reference to diabetes mellitus. Postgrad. Med. J. 47 (552), 654–659.
I Hisamitsu, K.K., Okano, T., Sakurai, Y., 1997. Glucose-responsive gel from phenylboronate polymer and poly(vinyl alcohol): prompt response at physiological pH through the interaction of boronate with amino group in the gel. Pharm. Res. 14 (3), 289–293.
J M Vigoureux, F.D., Girard, C., 1992. Supperresolution of near-field optical microscopy defined from properties of confined electromagnetic waves. Appl. Opt. 31 (6), 3036–3045.
J N Cambre, B.S.S., 2011. Biomedical applications of boronic acid polymers. Polymer 52, 4631–4643.
J R Adleman, H.A.E., Buse, K., Psaltis, D., 2006. Holographic grating formation in a colloidal suspension of silver nanoparticles. Opt. Lett. 31 (4), 447.
J Yan, G.S., Deeter, S., Wang, B., 2004. The relationship among pKa, pH, and binding constants in the interactions between boronic acids and diols—it is not as simple as it appears. Tetrahedron 60 (49), 11205–11209.
K Aslan, J.R.L., Geddes, C.D., 2004. Nanogold-plasmon-resonance-based glucose sensing. Anal. Biochem. 330, 145–155.
K Ino, T.F., Anzai, K., Iwase, M., Kogawa, K., Ogimoto, M., Ono, J., Takashi, A., Iida, M., Tamura, K., 2005. Serum Vitamin C levels in Type 2 diabetic nephropathy. Diabetes Care 28 (11), 2808–2809.
Kogelnik, H., 1969. Coupled-wave theory for thick hologram gratings. Bell Syst. Tech. J. 48 (9), 2909–2947.
Kumar, C., 2005. Clinical Medicine. Saunders Ltd..
M A Rodrigueza, M.S.M., Butlerb, J.J., 2000. Transmission properties of refractive index-shifted Bragg gratings. Opt. Commun. 117 (1–6), 251–257.
M Ellmerer, L.S., Sendlhofer, G., Wutte, A., Brunner, G.A., Trajanoski, Z., Skrabal, F., Wach, P., Pieber, T.R., 1998. Lactate metabolism of subcutaneous adipose tissue studied by open flow microperfusion. J. Endocrinol. Metab. 83 (12), 4394–4401.
M Matsumoto, T.S., Kondo, K., 2002. Selective adsorption of glucose on novel chitosan gel modified by phenylboronate. Sep. Purif. Technol. 29 (3), 229–233.
M Ozaki, J.K., Kawata, S., 2011. Surface-plasmon holography with white light illumination. Plasmon. Metamater. I 8455 (84550K-84551-84550K-84556).
M Rinaudo, G.P., Desbrieres, J., 1999. Influence of acetic acid concentration on the solubilization of chitosan. Polymer 40, 7029–7032.
M RTarkka, M.E.T., Brady, D.J., Schuster, G.B., 1994. Holgoraphic storage in a near-IR sensitive photochromic dye. Opt. Commun. 109 (1–2), 54–58.
M Uchida, A.T., 2010. Generation of electron beams carrying orbital angular momentum. Nat. Lett. 464, 737–739.
M-S Steiner, A.D., Wolfbeis, O.S., 2011. Optical methods for sensing glucose. Chem. Soc. Rev. 40 (11), 4805–4839.
McGarraugh, G., 2009. The chemistry of commercial continuous glucose monitors. Diabetes Technol. Ther. 11 (1), 17–24.
Michael S. Boyne, D.M.S., Kaplan, Joy, Saudek, Christopher D., 2003. Timing of changes in interstitial and venous blood glucose measured with a continuous subcutaneous glucose sensor. Am. Diabetes Assoc. 52 (11).
Monis, C., 2010. Hydrogel contact lenses. Chemical and Materials engineering. San Jose State University.

Mou, X., 2010. Long-term calibration considerations during subcutaneous microdialysis sampling in mobile rats. Biomaterials 31 (16), 4530.
N Hajdukova, P., Stepanek, J., Spirkova, M., 2007. Chemically reduced and laser-ablated gold nanoparticles immobilized to silanized glass plates: Preparation, characterization and SERS spectral testing. Colloids Surf. A, Physicochem. Eng. Asp. 301 (1–3), 264.
N R Panyala, E.M.Pa-Mn, Havel, J., 2008. Silver or silver nanoparticles: a hazardous threat to the environment and human health? J. Appl. Biomed. 6, 117–129.
Oliver, N.S., 2009. Glucose sensors: a review of current and emerging technology. Diabetic Med. 26 (3), 197.
WHOrganisation. 2013 Diabetes. .
P Rossetti, J.B., Vehi, J., Fanelli, C.G., 2010. Estimating plasma glucose from interstitial glucose: the issue of calibration algorithms in commercial continuous glucose monitoring devices. Sensors 10 (12), 10936–10952.
P Šmíd, H.H., Keprt, J., 2004. Dichromated gelatin and its importance for optical hologram recording. Czechoslov. J. Phys. 54 (12), 1461–1472.
R K Shervedani, M.B., 2008. Electrochemical characterization of in situ functionalized gold cysteamine self-assembled monolayer with 4-formylphenylboronic acid for detection of dopamine. Electroanalytics 20, 5.
Reem Smoum, A.R., Srebnik, Morris, 2006. Chitosan – pentaglycine – phenylboronic acid conjugate: a potential colon-specific platform for calcitonin. Bioconjugate Chem. 17 (4), 1000–1007.
Regittnig, W., 2003. Assessment of transcapillary glucose exchange in human skeletal muscle and adipose tissue. Am. J. Physiol.: Endocrinol. Metab. 285 (2), E241.
S Jin, Y.C., Reid, S., Li, M., Wang, B., 2009. Carbohydrate recognition by boronolectins, small molecules, and lectins. Pharma. Med. Chem. 30 (2), 171–257.
S Kabilan, A.J.M., Sartain, F.K., Lee, M.C., Hussain, A., Yang, X., Blyth, J., Karangu, N., James, K., Zeng, J., Smith, D., Domschke, A., Lowe, C.R., 2005. Holographic glucose sensors. Biosens. Bioelectronics 20 (8), 1602–1610.
S Kabilan, J.B., Lee, M.C., Marshall, A.J., Hussain, A., Yang, X.P., Lowe, C.R., 2004. Glucose-sensitive holographic sensors. Mol. Recognit. 17, 3.
S P Nichols, A.K., Storm, W.L., Shin, J.H., Schoenfish, M.H., 2013. Biocompatible materials for continuous glucose monitoring devices. Chem. Rev. 113 (4), 2528–2549.
S Vaddiraju, D.J.B., Tomazos, I., Jain, F.C., Papadimitrakopoulos, F., 2010. Technologies for continuous glucose monitoring: current problems and future promises. J. Diabetes Sci. Technol. 4 (6), 1540–1562.
Sartain, F.K., 2008. Complexation of l-lactate with boronic acids: a solution and holographic analysis. Chem.-A Eur. J. 14 (13), 4060.
Saxby G., 1994. Practical holography.
Saxby, G., 2004. Practical Holography. Taylor & Francis.
Springsteen, G., 2002. A detailed examination of boronic acid–diol complexation. Tetrahedron 58 (26), 5291.
T Kawasaki, H.A., Yamanouchi, T., 2002. Increased fructose concentrations in blood and urine in patients with diabetes. Diabetes Care 25 (2), 353–357.
T Konno, K.I., 2007. Temporal and spatially controllable cell encapsulation using a water-soluble phospholipid polymer with phenylboronic acid moiety. Biomaterials 28 (10), 1770–1777.
T N Smirnova, L.M.K., Kutsenko, A.S., Sakhno, O.V., Stumpe, J., 2009. The fabrication of periodic polymer/silver nanoparticle structures: in situ reduction of silver nanoparticles from precursor spatially distributed in polymer using holographic exposure. Nanotechnology 20 (40), 1–10.
Takumi Sannomiya, T.E.B., Hafner, Christian, Heuberger, Manfred, Vörös, Janos, 2010. Optical sensing and determination of complex reflection coefficients of plasmonic structures using transmission interferometric plasmonic sensor. Rev. Sci. Instrum. 81 (5), 053102–053109.
Vezouviou, E., 2013. A near Infrared holographic glucose sensor for diabetes management. Chemical Engineering and Biotechnology. University of Cambridge.
Wu Z, Z.S., Zhang, X., Shu, S., Chu, T., Yu, D., 2011. Phenylboronic acid grafted chitosan as a glucose-sensitive vehicle for controlled insulin release. J. Pharmaceutical Sci. 100 (6), 2278–2286.
X Hong, E.A.H.H., 2012. Contribution of gold nanoparticles to the signal amplification in surface plasmon resonance. Analyst 137, 4712–4719.
X Yang, X.P., Blyth, J., Lowe, C.R., 2007. Towards the real-time monitoring of glucose in tear fluid: holographic glucose sensors with reduced interference from lactate and pH. Biosens. Bioelectron. 23 (6), 899–905.
Xiaoping Yang, M.-C.L., Sartain, Felicity, Pan, Xiaohan, Lowe, Christopher R., 2006. Designed boronate ligands for glucose-selective holographic sensors. Chem.- A Eur. J. 12 (33).
Y Asantewaa, J.A., Burley, J.C., Billa, N., Roberts, C.J., 2013. Correlating physicochemical properties of boronic acid-chitosan conjugates to glucose adsorption sensitivity. Pharmaceutics 5, 69–80.
Y Pan, S.N., Leifert, A., Fischler, M., Wen, F., Simon, U., Schmid, G., Brandau, W., Jahnen-Dechent, W., 2007. Size-dependent cytotoxicity of gold nanoparticles. Small Nano Micro 3 (11), 1941–1949.